NUKLEONIKA 2022;67(1):XX–XX
doi: 10.2478/nuka-2021-0034

ORIGINAL PAPER

sciendo

Studies on water transport in quasi two-dimensional porous systems using neutron radiography

Izabela M. Fijał-Kirejczyk, Massimo Rogante, Jacek J. Milczarek, Joanna Żołądek-Nowak, Zdzisław Jurkowski, Jan Żołądek, Dariusz Rusinek

Abstract. The spontaneous wetting and drying of flat porous samples of linen, cotton and synthetic textiles were studied using dynamic neutron radiography (DNR). The progress of the wetting process of the media was delineated from the obtained neutron dynamical radiography images. The results of the investigation reveal a non-classical behaviour of kinetics of wicking of these materials. The character of the wetting kinetics is discussed in terms of the fractal character of the tortuosity of fabric capillaries.

Keywords: Water transport • Drying • Fractal • Neutron radiography • Wettability • Wicking • Wetting

Introduction

The studies on the transport of liquid in porous materials can help in the estimation of some model characteristics such as the effective size of the pores and wettability (effective wetting angle) of the porous systems used for wicking by the liquid of interest [1–7]. The studies on wetting are usually performed on bulk samples with most of their lateral surfaces covered with impermeable layers which preclude the evaporation of the liquid [8, 9]. Nevertheless, there are some porous systems of practical interest having the natural form and wicking features depending on their shapes. Due to their practical importance, the liquid transport in these systems, such as fabrics, tissues and paper sheets deserves special attention [1, 2]. Regarding the small thickness of sheets of those items as compared to their length and width, the systems can be considered quasi two-dimensional although embedded in three--dimensional environments. Naturally, such systems cannot be protected against evaporation by coating their surfaces with some evaporation averting agents without substantial change in their properties or environmental conditions of the process. In wetting studies of such samples, the evaporation of the wetting liquid is an important factor that cannot be ignored as an important process accompanying the wicking. It is obvious that the interest in water transport in quasi-2D samples comes from many branches of technology such as the textile and garment industry [1, 2], moisture management [6], packaging and printing technology [7, 10].

I. M. Fijał-Kirejczyk✉, J. J. Milczarek, J. Żołądek-Nowak, Z. Jurkowski, J. Żołądek, D. Rusinek
National Centre for Nuclear Research
Andrzeja Sołtana 7 Str., 05-400 Otwock-Świerk, Poland
E-mail: izabela.fijal-kirejczyk@ncbj.gov.pl

M. Rogante
Rogante Engineering Office
Contrada San Michel 61, 62012 Civitanova Marche
Italy

Received: 23 June 2020
Accepted: 10 September 2021

Water transport through various systems has attracted the interest of modern imaging science for many years. The overwhelming contribution has been provided by magnetic resonance imaging [10, 11] and X-ray computed tomography [11, 12]. The wide application of both techniques stems from the rapid development and availability of medical scanners. The third method, in use for almost 30 years, has been brought about by dynamic thermal neutron radiography (TNR).

The dynamic neutron radiography (DNR) [13–15] has been used for decades in quantitative investigations of transport processes of hydrogenous liquids in porous media [5, 16–19]. The technique allows not only for direct observation of wetting and drying fronts but provides also a suitable tool for quantitative studies of wetting and drying kinetics. The spontaneous water transport processes have been investigated with DNR in rigid and loose porous systems [5, 9, 15, 16]. Examples of the kinetics conforming to the classical diffusion equation as well as cases of non-classical or anomalous behaviour in wetting and drying processes have been delineated with DNR [5, 16, 17, 19]. So far only optical imaging was applied in studies of wicking in single sheets of fabrics [4]. The present study describes and proves that the DNR technique is sensitive enough to reveal the characteristics of water transport kinetics in flat samples of approximately 0.2–0.4 mm thickness which contain a minute quantity of water with its surface density not exceeding a few dozens of milligrams per square centimetre.

Experimental procedure

Three samples of different fabrics woven from linen, cotton and synthetic fibres were studied. The fabric samples of the rectangular shape of ~30 mm wide and ~130 mm long were stretched vertically on an aluminium or PMMA (Plexiglas) frame (Fig. 1). The thicknesses of the linen, cotton and synthetic fabric samples were 0.26 mm, 0.36 mm and 0.37 mm, respectively. The flat side of the sample was mounted parallel to the face of the detector screen. In the wetting experiment, the lower end of the sample was made to wet by dipping in water in an aluminium container. The system was housed in a thermal cell and the temperature was stabilized at 30(±0.5)°C. Drying of the samples was studied for initially almost uniformly water-saturated samples located vertically at the similar arrangement as in wetting studies in the drying tunnel at the temperature of 60(±2)°C of the flowing air.

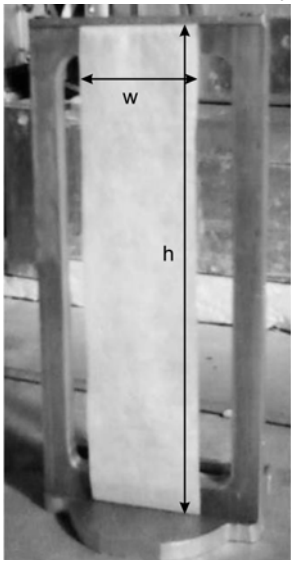

Fig. 1. A picture of the fabric sample spanned on the aluminium frame. The w and h denote the sample width and length, respectively.

The TNR images were obtained using a standard DNR facility (NGRS) installed at the 30 MW research nuclear reactor MARIA located at the National Centre for Nuclear Research at Otwock-Świerk, Poland. The operating principle of the system is common for every radiography station – radiations that pass through the sample reach the scintillator screen where they are detected and transformed into visible light and then recorded with an optical camera. In our system, a thermal neutron beam from the nuclear reactor is directed to the sample perpendicularly to its flat surface. The neutron-sensitive screen is monitored by a digital camera that registers the images formed by the light emitted. The amount of light produced with the neutrons reaching the screen is proportional to the number of neutrons hitting the screen in the area corresponding to the given camera pixel. The NGRS system consists of neutron beam collimators, designed to be fitted with a 25 cm × 25 cm size NDg (6Li:ZnS:Cu, Al, Au) scintillation screen of Applied Scintillation Technologies, a mirror, optical zoom lenses and highly sensitive 1280 × 1024 pixels Hamamatsu ORCA ER CCD camera operated under the HiPic (Hamamatsu Photonics) software. In the experimental setup (Fig. 2), the sample could be positioned in a thermal cell or a drying tunnel. The thermal cell was a closed box with an aluminium wall of 250 mm × 130 mm × 350 mm and the drying tunnel was an open tube of 10 cm in diameter. In effect, the sample to detector screen distance L_s was about 80 mm. The exposure time of 1.5 s was applied which was sufficient for the size and composition of the objects studied. The L/D ratio of source-to-detector distance (L) and collimator inlet diameter (D) was 160. The distance of the neighbouring pixels corresponds to 0.13 mm, and the effective spatial resolution obtained in TNR radiographs was 0.25 mm [16, 18, 19]. Images were registered, displayed online and stored in a dedicated computer system for subsequent analysis. Before discussion of the spatial and temporal variations in brightness at any pixel, the registered neutron images were corrected for dark current (J_{bc}) com-

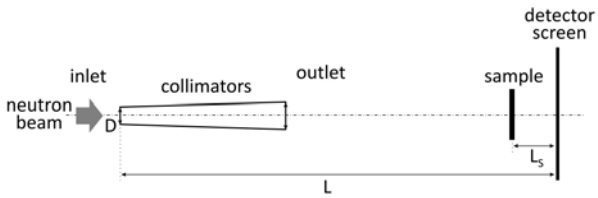

Fig. 2. The spatial arrangement of the sample position in the NGRS radiography facility.

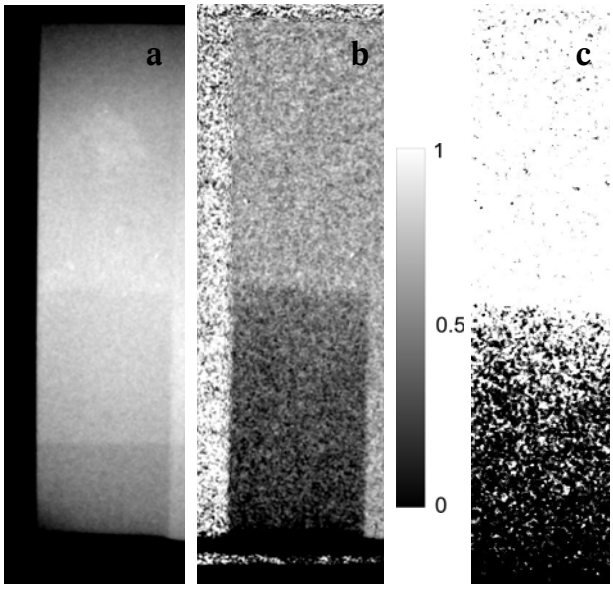

Fig. 3. The neutron images of wetting of synthetic fabric sample (a) before processing, (b) after subtraction of the black current and division by the dry sample image (with linear greyscale), (c) after reduction of the greyscale, histogram stretching and binarization.

ponent and neutron beam fluctuations factor (f). The brightness (B_w) which can be attributed to the water content, was determined as

$$B_w = f\frac{J_w - J_{bc}}{J_d - J_{bc}} \tag{1}$$

where J_w and J_d denote the brightness for the image of the sample with water and dry one, respectively. The beam fluctuation factor was determined for each image as the inverse ratio of average brightness of the carefully chosen image region far away from the sample representation on the picture to the brightness of the same region for the dry sample image and varied between 0.96 and 1.04. The mathematical operations on images were performed with the ImageJ software package [20].

Strong scattering of thermal neutrons on hydrogen nuclei abundant at the wetted part of the sample removes a substantial fraction of the neutrons from the incident beam producing dark regions in the neutron images of the sample. The darker regions of the image correspond to the smaller number of neutrons impinging on the screen at the given pixel. It was also physically verified in the samples that more water is contained in regions corresponding to the darker regions of the image (Fig. 3). It should be noted that the wetting front was not visible with the unaided eye on unprocessed images (Fig. 3a). For presentation purposes, the registered images (Fig. 3a) were processed by the application of black current subtraction and division by the dry sample image (Fig. 3b) and finally by the greyscale reduction and histogram stretching to produce binary pictures (Figs. 3c and 4). The procedure clearly revealed the water transport within the samples.

For quantitative examination of the water distribution within the samples, the distribution of the brightness B_w on the obtained images was studied. According to the Beer–Lambert law [9, 13, 15, 16], the amount of water contained at any location of the sample is proportional to the optical density of the corresponding pixel in the image. The amount of water present is proportional to the optical density D_{opt} calculated as the negative logarithm of the brightness B_w (Eq. (1)) and is given by

$$D_{\text{opt}} = -\ln B_w. \tag{2}$$

Natural inhomogeneity of fabric samples produces an erratic occurrence of the dark regions and borders (Figs. 3c and 4) during wetting. To smooth the dependence of the optical density on the distance from the water immersed end of the sample, the average distribution of water along the wetted sample was calculated by averaging the brightness on the segments perpendicular to the length of the sample (Fig. 5). The wetting front position d was determined from that averaged optical density dependence on the distance x from the water immersed end. Regarding natural fluctuations in brightness and subsequently the optical density it was assumed that the front position corresponds to the average optical density threshold equal to 0.01 (Fig. 5).

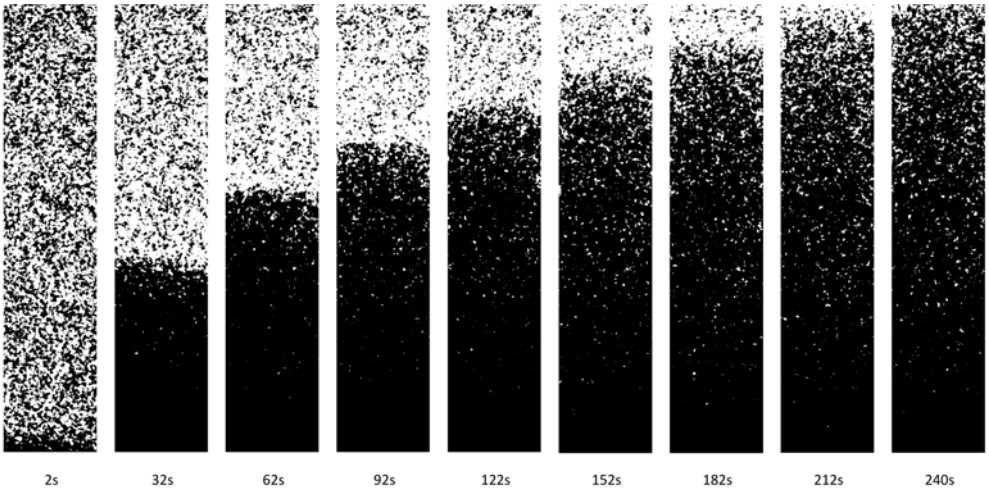

Fig. 4. Binarized (to reveal the waterfront for the naked eye) neutron radiography images sequence delineating the water wetting of a synthetic fabric. The black and white areas correspond to the water-saturated and dry regions, respectively. The values at the bottom indicate the time elapsed since the moment of contact of the sample lower end with water.

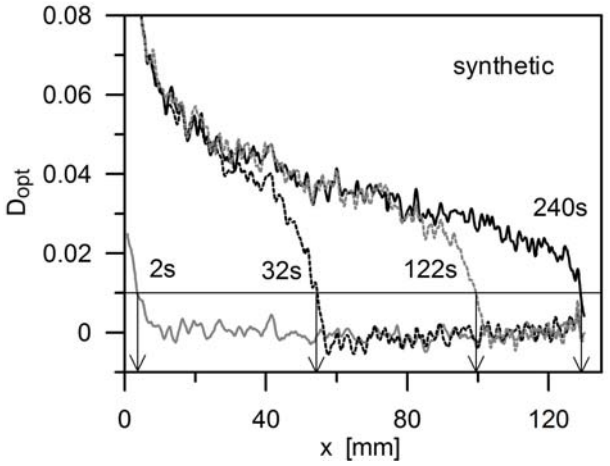

Fig. 5. The dependence of the optical density (negative logarithm of the average brightness) on the distance from the water-immersed, lower end of the sample of synthetic fabric. The solid horizontal line represents the assumed threshold value of 0.01 that determines the wetting front position.

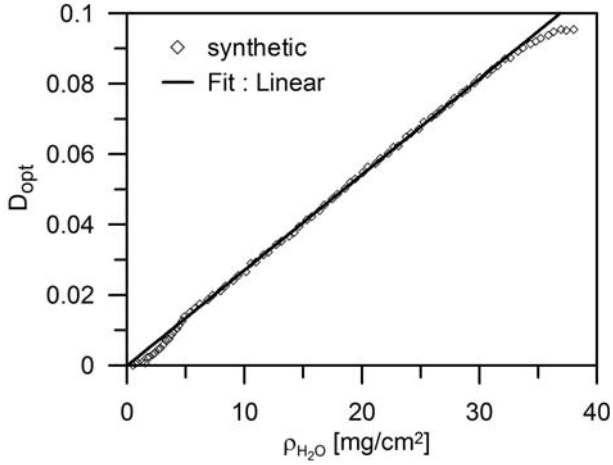

Fig. 6. The dependence of the average optical density of the sample image on the average surface mass density of the water for drying of the synthetic fabric.

The profiles of the optical density along the sample long axis exhibit a very fast drop in the lowest part of the sample indicating a very large gradient in the amount of water in the region close to the wetted end. Then the water content decreases almost linearly with distance from the lower end to reach the wetting front region characterized by a marked drop in optical density. It should be noted that the initial region of the high gradient of water content and linear decrease part of this dependence persist even after complete saturation of the sample with water was reached. The former feature should be attributed to a kind of meniscus formed at the water immersed part of the sample whereas the linear part is due to a dynamical equilibrium between the evaporation and capillary transport processes.

Despite its important contribution to the wicking of textile samples, the effect of inherent evaporation of water from open surfaces of samples has not been studied in detail. However, in this work, the evaporation from samples was to some extent suppressed by the presence of vapour supplied from the open surface of water filling the lower container during wetting in the thermal cell.

Analysis and discussion

The analysis of the drying experiments yielded an almost direct proportionality between the average optical density D_{opt} of the image of the sample and the sample mass m. This feature allows to express the local surface density (dm/dS) of water mass in terms of the local optical density in the image of the sample (Fig. 6). Although the linearity of this dependence is perfect for most of the observed water surface density, the deviations from it are observed for the low water content samples as well as for water-saturated samples. The deviations from linearity for the advanced phase of drying with small water content can be attributed to the patchy structure of the sample which consists of neighbouring wet and almost dry regions. It is known that the scattered from the wet regions neutrons reaching the detector enhance the brightness of the image reducing the optical density [13–15, 21–23]. At the final phases of drying the dry regions dominate so the average optical density is not proportional to the amount of water in the sample. In effect, we found that in drying the average brightness is greater than predicted from the linear dependence of brightness on water surface density yielding a spoon-like behaviour in the low mass region of the optical density vs. mass density plot (Fig. 6). At beginning of drying of water-saturated sample, the incoherent scattering of neutrons by hydrogen atoms reduces the average optical density of images due to the presence of the scattered neutron component. The effect of the scattered neutrons illuminating the detector screen is substantial in the quantification of the amount of water in thick samples placed close to the detector [21–23]. However, we assumed that due to large sample to detector distance as well as a small surface density of water in the samples the contribution of the scattering neutrons is not crucial for the determination of the variations of the water content along the samples and the wetting front position [24–26]. The amount of water is directly connected to the thickness of the water layer [9, 13, 15, 16]. The thickness of the layer cannot be studied directly with DNR because of the limited time and spatial resolution of the technique but one should expect that the X-ray microtomography could yield valuable results for this variable [26].

The wetting rate was described by the time dependence of the wetting front position (Fig. 7). In most cases studied so far one finds that this dependence can be approximated with the power law: $d(t) \sim t^{\alpha}$ [4, 7, 9, 10]. In the present study it was found that exponent a was 0.35, 0.41, and 0.43 (± 0.005) for cotton, linen and synthetic fabric, respectively (Fig. 7). These values are distinctly different from the classical value of 0.5 predicted by the capillary suction theories of straight tubes and observed for many bulk porous systems [9, 18, 19, 27]. Moreover, it indicates a significant reduction in

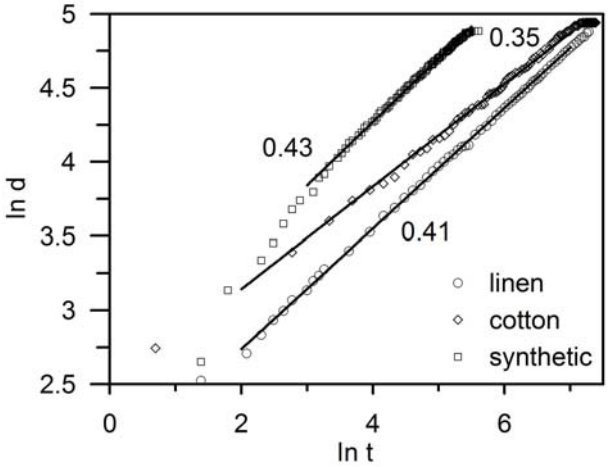

Fig. 7. The logarithmic plot of the wetting front distance from the water immersed end of the cotton, linen and synthetic fabrics on time. The numbers are the fitted values of α exponents as explained in the text.

the wetting front velocity for imbibition proceeding with accompanying evaporation in comparison to that for the process evolving without substantial evaporation.

The problem of the non-classical dependence of the wetting height on time has been discussed recently in terms of the tortuous path of the capillaries formed within studied material [27, 28]. Within that model, the system consists of bundles of tortuous tubes. It has been pointed out that the actual path of the water is much larger than the straight-line distance measured from the water-dipped end of the sample [27, 28]. It has been shown [28] that if there is a fractal scaling relation between the diameter λ and actual length L_f of the capillary:

$$L_f = \lambda^{1-D_T} L_s^{D_T} \tag{3}$$

with D_T denoting the fractal dimension and L_s representing the ideal straight line capillary length, then the time dependence of the straight line distance of the wetting front is determined by

$$L_s = At^{1/2D_T} \tag{4}$$

where according to Eq. (17) of the [28] the proportionality constant A depends on the capillary diameter, the fractal dimension, the liquid viscosity and surface tension as well as the liquid-capillary wall wetting angle.

The fractal dimension determined from the results of our measurements based on such reasoning yields the D_T equal to 1.43, 1.22, and 1.16 for cotton, linen and synthetic textile, respectively. These values are quite reasonable since they differ only slightly from the straight-line dimension of 1. Moreover, these values support the quasi two-dimensional description of the systems since they are significantly <2. The capillary tortuosity stems from the erratic deviations of the capillary long axis from the straight line connecting capillary ends. Nevertheless, all the system capillaries are contained within the system plane.

In some considerations [3, 9, 29, 30], a universal description of spontaneous wetting has been

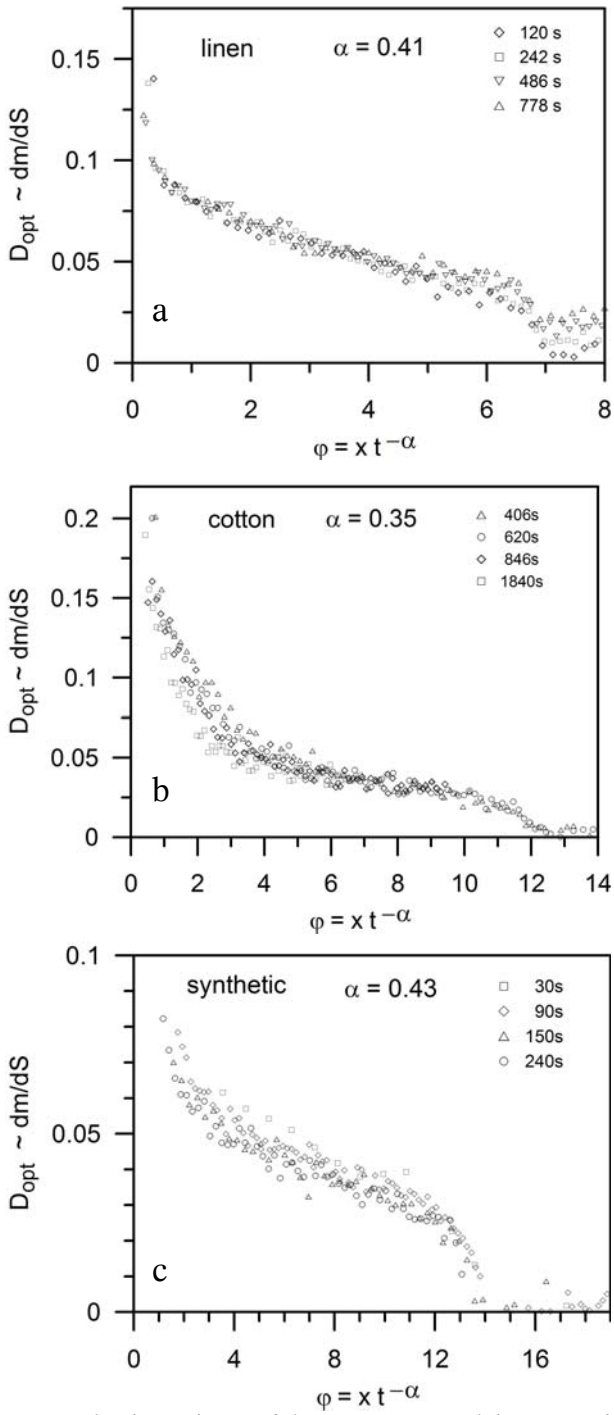

Fig. 8. The dependence of the average optical density and the generalized variable $\varphi = xt^{-\alpha}$ for wetting of linen (a), cotton (b) and synthetic (c) fibre textile.

suggested based on the assumption of the anomalous diffusion mechanism of wetting of stochastic systems. Various anomalous diffusion equations have been invoked leading to the conclusion that the water distribution along the sample main axis should coalesce to a single curve if plotted vs. the reduced variable $\varphi = xt^{-\alpha}$, where α is the power-law exponent of wetting front position on time, where x denotes the distance from the water immersed end of the sample [3, 9, 29, 30]. We found that in our study the distribution of the optical density along the sample axis almost converges to one curve only

in some plot regions when plotted vs. the $\varphi = xt^{-\alpha}$ variable (Fig. 8). The acceptable coincidence of the normalized profiles is found only for the linen fabric (Fig. 8a). The poorest convergence is found for the synthetic fabric (Fig. 8c). The large initial region of steep descent of amount of water with the distance x from the water immersed end of the sample was observed for cotton and synthetic fabrics (Fig. 8b,c). Nevertheless, two regions with different slopes of the dependence of the amount of water on φ variable have been revealed for the larger distances from the lower end of the sample. The first is found for medium distances and the very steep second region is due to the wetting front. We conclude that the expected coalescence of the data to one universal curve is not satisfactory enough to proceed with further analysis for any of the investigated systems.

Summary

In the present study, it is proved that the DNR is useful in quantitative studies on wetting and drying of very thin objects containing small amounts of water. The results indicate that the spontaneous wetting of such objects can be described in terms of the fractal structure of the tortuous capillaries model which is consistent with the assumption of quasi two-dimensional nature of those systems. The results suggest that there is no universal dependence of the water distribution within quasi two-dimensional systems which could support the application of anomalous diffusion approach to all such systems.

ORCID

I. M. Fijał-Kirejczyk https://orcid.org/0000-0002-0974-5880
J. J. Milczarek https://orcid.org/0000-0002-8228-3184
M. Rogante https://orcid.org/0000-0002-6846-0826
D. Rusinek http://orcid.org/0000-0002-7421-5595
J. Żołądek http://orcid.org/0000-0001-8136-5594
J. Żołądek-Nowak https:// orcid.org/0000-0002-1632-7302

References

1. Azeem, M., Boughattas, A., Wiener, J., & Havelka, A. (2017). Mechanism of liquid water transport in fabrics: A review. *Vlákna a textil (Fibres and Textiles)*, *24*(4), 58–65. http://vat.ft.tul.cz/2017/4/VaT_2017_4_10.pdf.
2. Lei, M., Li, Y., Liu, Y., Ma, Y., Cheng, L., & Hu, Y. (2020). Effect of weaving structures on the water wicking-evaporating behavior of woven fabrics. *Polymers*, *12*, 422. DOI: 10.3390/polym12020422.
3. de Azevedo, E. N., Alme, L. R., Engelsberg, M., Fossum, J. O., & Dommersnes, P. (2008). Fluid imbibition in paper fibres: Precursor front. *Phys. Rev. E*, *78*, 066317. DOI: 10.1103/PhysRevE.78.066317.
4. Benloufa, S., Fayala, F., & Nasrallah, S. B. (2008). Capillary rise in micro pores of jersey knitting structure. *J. Eng. Fiber Fabr.*, *3*(3), 47–54. http://www.jeffjournal.org/papers/Volume3/JEFF08-00007R1Benltoufa.pdf.
5. Abd, A. E. -E., Czachor, A., Milczarek, J. J., & Pogorzelski, J. (2005). Neutron radiography studies of water migration in construction porous materials. *IEEE Trans. Nucl. Sci.*, *52*(1), 299–304. DOI: 10.1109/TNS.2005.843642.
6. Hamdaoui, M., Achour, N. S., & Nasrallah, S. B. (2014). The influence of woven fabric structure on kinetics of water sorbtion. *J. Eng. Fiber Fabr.*, *9*(1), 101–106. http://www.jeffjournal.org/papers/Volume9/V9I1.12.M.Hamdaoui.pdf.
7. Samyn, P. (2013). Wetting and hydrophobic modification of cellulose surfaces for paper applications. *J. Mater. Sci*., *48*(19), 6455–6498. DOI: 10.1007/s10853-013-7519-y.
8. Xie, Y., Hill, C. A. S., Jalaludin, Z., Curling, S. F., Anandjiwala, R. D., Norton, A. J., & Newman, G. (2011). The dynamic water vapour sorption behaviour of natural fibres and kinetic analysis using the parallel exponential kinetics model. *J. Mater. Sci*., *46*(2), 479–489. DOI: 10.1007/s10853-010-4935-0.
9. Abd, A. E., & Milczarek, J. J. (2004). Neutron radiography study of water absorption in porous building materials: anomalous diffusion analysis. *J. Phys. D-Appl. Phys*., *37*(16), 2305–2313. DOI: 10.1088/0022-3727/37/16/013.
10. Leisen, J., Hojjatie, B., Coffin, D. W., & Beckham, H. W. (2001). In-plane moisture transport in paper detected by magnetic resonance imaging. *Dry. Technol.*, *19*(1), 199–206. DOI: 10.1081/DRT-100001361.
11. Perré, P. (2011). A review of modern computational and experimental tools relevant to the field of drying. *Dry. Technol.*, *29*(13), 1529–1541. DOI: 10.1080/07373937.2011.580872.
12. Escalona, I., Jomaa, W., Olivera-Fuentes, C., Crine, M., & Leonard, A. (2010). Convective drying of gels: Comparison between simulated and experimental moisture profiles obtained by X-ray microtomography. *Dry. Technol.*, *28*(5), 644–650. DOI: 10.1080/07373931003788734.
13. Domanus, J. C. (Ed.). (1992). *Practical neutron radiography*. Dordrech: Kluwer Academic Publishers. (EUR-14424).
14. Strobl, M., Manke, I., Kardjilov, N., Hilger, A., Dawson, M., & Banhart, J. (2009). Advances in neutron radiography and tomography. *J. Phys. D-Appl. Phys*., *42*(24), 243001. DOI: 10.1088/0022-3727/42/24/243001.
15. Anderson, I. S., McGreevy, R. L., & Bilheux, H. Z. (Eds.). (2009). *Neutron imaging and applications*. Berlin: Springer. DOI: 10.1007/978-0-387-78693-3.
16. Milczarek, J. J., Czachor, A., Abd, A. E., & Wiśniewski, Z. (2005). Dynamic neutron radiography observations of water migration in porous media. *Nucl. Instrum. Methods Phys. Res. Sect. A-Accel. Spectrom. Dect. Assoc. Equ.*, *542*(1/3), 232–236. DOI: 10.1016/j.nima.2005.01.105.
17. Cmiel, K., Milczarek, J. J., Bam, L. C., Fijał-Kirejczyk, I. M., Jurkowski, Z., & Żołądek, J. (2013). Drying kinetics of particulate corundum layers. *Acta Phys. Pol. A*, *124*, 1029–1033. DOI: 10.12693/APhysPolA.124.1029.
18. Fijał-Kirejczyk, I. M., Milczarek, J. J., Żołądek-Nowak, J., de Beer, F. C., Radebe, M. B., & Nothnagel, G. (2012). Application of statistical image analysis in

quantifcation of neutron radiography images of drying. *Acta Phys. Pol. A*, *122*, 410–414. DOI: 10.12693/APhysPolA.122.410.

19. Fijał-Kirejczyk, I. M., Milczarek, J. J., de Beer, F. C., Radebe, M. B., Nothnagel, G., & Żołądek-Nowak, J. (2012). Thermal neutron radiography studies of drying of rectangular blocks of wet mortar. *Nukleonika*, *57*(4), 529–535. http://www.nukleonika.pl/www/back/full/vol57_2012/v57n4p529f.pdf.
20. Rasband, W. S. (1997–2018). ImageJ [computer software]. Bethesda, Maryland, USA: National Institutes of Health. https://imagej.nih.gov/ij/.
21. Lehmann, E. H., Vontobel, P., & Kardjilov, N. (2004). Hydrogen distribution measurements by neutrons. *Appl. Radiat. Isot.*, *61*, 503–509. DOI: 10.1016/j.apradiso.2004.03.075.
22. Kardijlov, N., de Beer, F., Hassanein, R., Lehmann, E., & Vontobel, P. (2005). Scattering corrections in neutron radiography using point scattered functions. *Nucl. Instrum. Methods Phys. Res. Sect. A-Accel. Spectrom. Dect. Assoc. Equ.*, *542*, 336–341. DOI: 10.1016/j.nima.205.01.159.
23. Deinert, M. R., Parlange, J. -Y., Steenhuis, T., Throop, J., Ünlü, K., & Cady, K. B. (2004). Measurement of fluid contents and wetting front profiles by real-time neutron radiography. *J. Hydrol.*, *290*, 192–201. DOI: 10.1016/j.hydrol.2003.11.018.
24. Kim, F. H., Penumadu, D., & Hussey, D. S. (2012). Water distribution variation in partially saturated granular materials using neutron imaging. *J. Geotech. Geoenviron. Eng.*, *138*(2), 147–154. DOI: 10.1061/(ASCE)GT.1943-5606.0000583.
25. Kang, M., Bilheux, H. Z., Voisin, S., Cheng, C. L., Perfect, E., Horita, J., & Warren, J. M. (2013). Water calibration measurements for neutron radiography: Application to water content quantification in porous media. *Nucl. Instrum. Methods Phys. Res. Sect. A-Accel. Spectrom. Dect. Assoc. Equ. 708*, 24–31. DOI: 10.1016/j.nima.2012.12.112.
26. Parada, M., Vontobel, P., Rossi, R. M., Derome, D., & Carmeliet, J. (2017). Dynamic wicking process in textiles. *Transp. Porous Media*, *119*, 611–632. DOI: 10.1007/s11242-017-0901-5.
27. Cai, J., & Yu, B. (2011). A discussion of the effect of tortuosity on the capillary imbibition in porous media. *Transp. Porous Media*, *89*(2), 251–253. DOI: 10.1007/s11242-011-9767-0.
28. Cai, J. -C., Yu, B. -M., Mei, M. -F., & Luo, L. (2010). Capillary rise in a single tortuous capillary. *Chin. Phys. Lett.*, *27*(5), 054701. DOI: 10.1088/0256-307X/27/5/054701.
29. Metzler, R., & Klafter, J. (2000). The random walk's guide to anomalous diffusion: a fractional dynamics approach. *Phys. Rep.*, *339*, 1–77. DOI: 10.1016/S0370-1573(00)00070-3.
30. de Azevedo, E. N., de Sousa, P. L., de Souza, R. E., Engelsberg, M., de Miranda, M. N. do N., & Silva, M. A. (2006). Concentration dependent diffusivity and anomalous diffusion: A magnetic resonance imaging study of water ingress in porous zeolite. *Phys. Rev. E*, *73,* 011204. DOI: 10.1103/PhysRevE.73.011204.